Modelling tsunamis in the Eastern Mediterranean Sea. Application to the Minoan Santorini tsunami sequence as a potential scenario for the biblical Exodus

R. Periáñez *, J.M. Abril

Dpto. Física Aplicada I, ETSIA, Universidad de Sevilla, Ctra. Utrera km 1, 41013 Seville, Spain

A B S T R A C T

A numerical model which simulates the propagation of tsunamis in the Eastern Mediterranean has been developed. Several tsunami sources have been considered: earthquakes associated to geological faults, submarine landslides, entry of pyroclastic flows into the sea and the collapse of a volcano caldera. The model has been applied to different past events for which historic data or previous simulations exist, to test its performance. Then it has been applied to simulate tsunamis triggered by the explosion of Santorini volcano (17th century BC) in the Aegean Sea. While the model accounts for run-ups in the Aegean coasts, it fails to explain the isochronous tsunamigenic deposits reported in eastern Sicily and the levantine coasts. A scenario of a sequence of intense tectonics strain release triggering a series of tsunamis could better fit the whole dataset. Thus, a submarine landslide at the Gulf of Sirte may explain the Augias megaturbidite and the sedimentary deposits reported in Augusta Bay (Sicily). Similarly, a sequential tsunami in the eastern Nile Delta may explain the tsunamigenic deposits found in Israel and Gaza. Considering the former coastline at 3500 years BP, it could also provide a plausible scenario for the biblical sea crossing related in the Exodus.

Keywords:
Numerical modelling
Eastern Mediterranean
Tsunamis
Landslide
Caldera collapse
Santorini
Nile Delta

1. Introduction

The geodynamics of the eastern Mediterranean is governed by the interactions between the Eurasian, African, Arabian and Anatolian plates, being the most relevant geophysical features the Rift of Suez, the Dead Sea shear zone and the Hellenic and Cyprus arcs (Barka and Reilinger, 1997; Mascle et al., 2000; Yolsal and Taymaz, 2012). This complex tectonic is responsible for intense earthquake and volcanism activity, triggering large tsunamis in the past (Hamouda, 2006; Novikova et al., 2011; Stiros, 2010; Yolsal and Taymaz, 2012). Consequently, it is an area prone to serious potential tsunami hazards (Lorito et al., 2008; Tinti et al., 2005).

The Minoan eruption of Thera (Santorini), also known as the Late Bronze Age (LBA) eruption, and dated around 1613 BC, was one of the largest Plinian eruptions on earth in the past 10,000 years. It has been related with the demise of the Minoan culture in the southern Aegean Sea, and also with the biblical plagues of Egypt preceding the exodus of Israelites. A summary of the phases of the Santorini eruption and tsunami generation can be found in Friedrich (2013) and Novikova et al. (2011). During the third phase, the caldera collapsed and massively thick (up to 55 m) pyroclastic flows entered into the sea, producing giant tsunami events. The final caldera collapse resulted in additional pyroclastic flows during the fourth phase. A pre-eruption earthquake (Cioni et al., 2000) could also have triggered a tsunami (Dominey-Howes, 2004).

This sequence of tsunamis left their fingerprint, identified through sedimentary deposits dated at the time of Santorini eruption, in a large area of the western Mediterranean: most of the coastlines of the Aegean Sea, with near-shore wave amplitudes on the order of 7–15 m along coastal Thera, SW Turkey and Crete (Novikova et al., 2011), but also Cyprus (where the site of Ayia Irini has been documented by Mészáros, 1978), the coastal area of Israel and Gaza (Goodman-Tchernov et al., 2009; Neev et al., 1987; Pfannenstiel, 1960) and the area of Augusta Bay, in eastern Sicily (De Martini et al., 2010, 2012). It is worth noting that in many cases, sedimentary deposits may not have been preserved, and other areas still remain unstudied. While results from tsunami models, which include the entry of pyroclastic flows and caldera collapse, are able to reasonably account for the estimated runups in the Aegean Sea coasts (Novikova et al., 2011; Ozel et al., 2011), they fail to generate waves which could explain the observed effects in other areas (e.g., the eastern Sicily and the Israel and Gaza coasts). This limitation is likely attributable to the fact that the Aegean Sea is a semi-enclosed water body, and the Hellenic arc, from Greece and Crete to Rhodes, acts as a physical barrier which dissipates most of the tsunami energy.

* Corresponding author at: Dpto. Física Aplicada I; ETSIA, Universidad de Sevilla; Ctra. Utrera km 1, DP 41013-Seville, Spain. Tel.: +954486473; fax: +954486436.
E-mail address: rperianez@us.es (R. Periáñez).

Moreover, Dominey-Howes (2004) reported results of a new geological investigation for LBA tsunami deposits at 41 coastal sites from Crete and Kos, where no terrestrial geological evidences of tsunamis were identified. The author also presented a critical review of the previously reported geological traces. He argues that there is insufficient evidence to demonstrate that any significant far-field tsunami could have propagated throughout the entire eastern Mediterranean. Particularly, a tsunami generated by the caldera collapse could not have propelled the floating pumice towards the coast of Israel, and, if transported by surface currents, the required time (about 6 weeks) would not agree with the arrival time of the tsunami. Dominey-Howes (2004) also argues that most caldera collapses are chaotic, occurring over an extended period of time (a few days or longer), and not instantaneously, which seriously limits their tsunamigenic potential.

Cita et al. (1996) and Cita and Rimoldi (1997), from the analysis of 54 deep sea sediment cores, and among other types of homogenites, provided empirical evidence of a 10–20 m thick megaturbidite in the Ionian Abyssal Plain (the so-called Augias megaturbidite) with an estimated volume of at least 11 km^3. They found some shallow-water bioclastic debris in the sand fraction, clearly displaced from the African shelf, most likely from the Gulf of Sirte (Shiki and Cita, 2008). From ^{14}C dating (Hieke, 1984; Troelstra, 1987) and the analysis of sediment accumulation rates, constrained by the sapropel layer marker, the authors found that this megaturbidite was isochronous with the Santorini eruption (Cita et al., 1996). Hieke and Werner (2000) re-evaluated the volume of the mobilized sediments to a minimum of 65 km^3, derived from the Gulf of Sirte (revealed by its high aragonite content). More recently, Polonia et al. (2013) published results on radiocarbon ages obtained from planktonic foraminifera at different stratigraphic levels in two sediment cores that contained the entire homogenite. They concluded that the Santorini eruption might indeed have triggered mass failures in the central Mediterranean, but not the deposition of a megaturbidite. This last should be associated to the AD 365 Crete earthquake, with the mobilized sediments containing components from different sources, including the Malta escarpment and the Sicily Channel. It is worth noting that the two studied cores came from a location facing Malta and the Sicily Channel, and out of the area of the Augias megaturbidite depicted by Hieke and Werner (2000), as shown in Fig. 1 of Polonia et al. (2013).

The Santorini earthquake could have triggered a submarine landslide or gigantic turbidity currents in the African shelf around the Gulf of Sirte. Cita and Rimoldi (1997), basing upon the order of magnitude calculations, claimed that the Santorini tsunami wave speed could have been sufficient to induce erosion and liquefaction of the soft unconsolidated sediments. Nevertheless, detailed modelling results from Novikova et al. (2011) and from our present calculations, show low amplitudes for the tsunami waves in this area. But sediment liquefaction can be directly induced by seismic P-waves. Thus Cita et al. (1996) estimated that the pressure pulse induced by the P-waves was higher than 3.5×10^4 Pa (spontaneous liquefaction, under shallow water storm waves, occurs at 2.8×10^4 Pa). Several empirical relationships have been established between earthquake magnitude and distance for liquefaction in emerged lands (Galli, 2000; Papathanassiou et al., 2005) but with few empirical data exceeding distances larger than 100 km. Recent findings (Sigurdsson et al., 2006) suggested a re-evaluation of the VEI (Volcanic Explosivity Index) of the Santorini volcano explosion to 7.1, resulting then comparable to the 1815 eruption of Tambora in Indonesia, which released an energy equivalent to 800 Megatons.

The seismicity in the area as reported in the USGS National Earthquake Information Center catalogue (http://neic.usgs.gov/neis/epic/) since 1900 includes two earthquakes near the coasts of the Gulf of Sirte, with magnitudes of 7.1 (1935) and 5.1 (1988), and a large group with magnitudes over 5.0 in southwestern Crete and central Mediterranean. Whatever it was the triggering mechanism for such submarine landslide, if accepted to be isochronous with the Santorini event (within the involved dating uncertainties), the shift in the potential gravitational energy involved in the displacement of the most conservative estimate of 11 km^3 of solids from the African continental shelf to the Ionian Abyssal Plain, could have released an energy equivalent to several tens of Megatons, being able then to generate a secondary tsunami.

Stanley and Sheng (1986) first reported the evidence for the presence of ash ejected from the LBA Santorini explosion in sediment cores from the Eastern Nile Delta. This finding considerably extended the zone of confirmed ash fall. Trevisanato (2006a, 2006b, 2007) reported how six medical papyri described the effects of Santorini's volcanic ash, providing Egyptian parallels to the exodus biblical plagues.

Recent archaeological findings (Byers, 2006; Hoffmeier, 2005) provide new insight in the Exodus route and the location of the sea crossing. Thus, when the people of Israel left Peru-nefer (the ancient Avaris) they travelled southeast towards Succoth (in the nowadays Tell el-Maskhuta) and Etham. Then they turned back northwards, to Migdol, one of the military fortresses in the *Horus Way*, placed in the shoreline of a palaeo-lagoon opened to the Mediterranean Sea. The Tjaru bridge (close to the nowadays Qantara) should have been the only available pathway towards Sinai. It crossed the waterway that defined the eastern border, denoted *the dividing waters*, and connected the Gulf of Suez (whose shoreline extended to the north more than nowadays) with the Mediterranean through a large lacustrine system (the two Bitter Lakes, and the Timsah and Ballah lakes) and several transects of artificial canals. Thus, the waterbody that the Israelites crossed when leaving Egypt, called *yam suph*, *the Sea of Reeds*, should have been a large body of water in Egypt's eastern border. Although the chronology of the biblical Exodus has been controversial, the narrative could have been inspired by the major natural disasters that followed the LBA Santorini explosion.

Thus, the triggering mechanisms, the sequence, intensity and effects of the Minoan Santorini tsunamis seem to be far from being fully understood. Given the whole set of geological evidences of isochronous (within the involved uncertainties) tsunami deposits found in coastal areas, from Sicilia to Israel, and the Augias megaturbidite, it seems difficult to assume that a single event or a single tsunami source occurred. It is well known that the tectonic strain can be released in a series of large earthquakes, each one triggering the next, over a decadal time scale, what is usually termed as an *earthquake sequence* or an *earthquake storm* (Nur and Cline, 2000). A scenario in which the Santorini volcano explosion could have been the head or only a part of a sequence of intense tectonic strain release might better fit the whole situation described above, and has been denoted as a *tsunami sequence*.

The aim of this paper is to test this hypothesis through a modelling study of tsunamis in the eastern Mediterranean triggered by different mechanisms, including geological faults, submarine landslides, pyroclastic flows, and caldera collapse. This requires the development of numerical tools and their validation against several historical events and/or independent modelling exercises. The model is based on the 2D depth-averaged shallow water equations. It is fully non-linear and also allows run-up calculations. The model domain (Fig. 1) covers the central and eastern Mediterranean.

The model is briefly described in Section 2 and its application to past events is presented in Section 3. The Santorini tsunami sequence is investigated in Section 4. In particular, the potential origin of the Augias megaturbidite (Ionian Sea abyssal plain) as a result of a secondary or sequential tsunami is discussed in Section 4.1. The Nile delta deep-sea fan is a geologically active area, governed by salt tectonics and gravity gliding that have produced large-scale slope failures in the past. Here we will conduct a modelling exercise to study the potential effects of tsunamis generated by submarine landslides in the Delta along Israel and Gaza coasts, and to evaluate to what extent such a tsunami could conform to the biblical crossing of waters (Section 4.2).

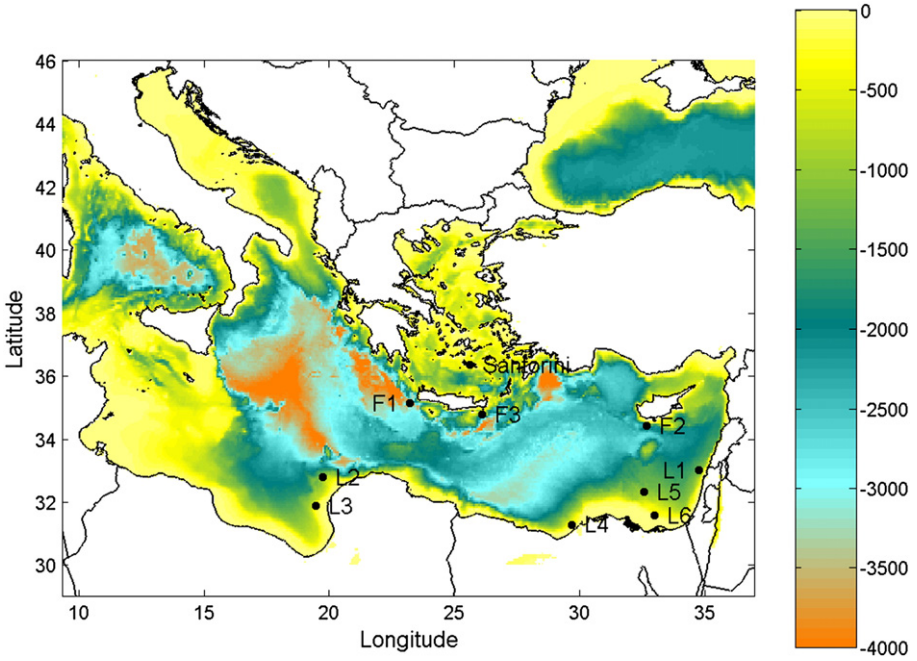

Fig. 1. Model domain. Water depths are given in m. All tsunami sources are presented. The center of the corresponding active fault, in the case of earthquake tsunamis (F1, F2 and F3), and the initial position of the slide front, in the case of landslides (L1 to L6), are drawn.

2. Model description

The tsunami propagation model is based on the 2D depth-averaged barotropic shallow water equations, which describe the propagation of surface shallow water gravity waves (see for instance Kowalik and Murty, 1993; Periáñez and Abril, 2013). The tsunami model, in the case of tsunamis generated by earthquakes, has been validated in south Iberia waters through the simulation of historic tsunamis as the Lisbon 1755, Algeria 1856 and Algeria 2003 tsunamis (Periáñez and Abril, 2013). The model has now been implemented in the eastern Mediterranean (Fig. 1) and new generation mechanisms have been incorporated: submarine landslides, pyroclastic flows and caldera collapse.

All the equations are solved using explicit finite difference schemes (Kowalik and Murty, 1993) with second order accuracy. In particular, the MSOU (Monotonic Second Order Upstream) is used for the advective non-linear terms in the momentum equations.

The computational domain extends from 9°20′E to 36°15′E and from 29°15′N to 46°N. It is presented in Fig. 1. Water depths have been obtained from the GEBCO08 digital atlas, available on-line, with a resolution of 30 s of arc both in longitude and latitude. Due to the CFL stability condition (Kowalik and Murty, 1993), time step for model integration was fixed as $\Delta t = 1$ s.

Boundary conditions have to be supplied. A gravity wave radiation condition (Herzfeld et al., 2011) is used for sea surface elevation along open boundaries, which is implemented in an implicit form. This condition avoids artificial wave reflections in open boundaries. A flood/dry algorithm is required since when the tsunami reaches the coast new wet or dry grid cells may be generated due to run-up or rundown. The numerical scheme described in Kampf (2009) has been adopted.

Four different tsunami sources are considered, which are briefly described below. They are earthquakes associated with geological faults, submarine landslides, entry of pyroclastic flows into the sea and the collapse of a volcano caldera. In all cases, the model is started from rest (zero water velocities over all the domain).

2.1. Tsunamis produced by earthquakes in geological faults

The vertical sea-floor deformation is considered as the initial condition for the tsunami calculation, which is the standard approach (see Lima et al., 2010; Sahal et al., 2009; Ioualalen et al., 2010 among many others). The sea-floor deformation produced by the earthquake is computed using the classical Okada formulae (Okada, 1985). Input for this equation is fault plane strike, rake, dip, slip, location, length and width, as well as seismic moment and rigidity.

2.2. Model for caldera collapse

In this case, the initial water level corresponds to the depth of the caldera formed. The initial water displacement is negative (i.e., downwards). This methodology has been successfully used in the past (Nomanbhoy and Satake, 1995; Novikova et al., 2011) and thus it has been adopted in this work.

2.3. Submarine landslides

The methodology of Harbitz (1992) and Cecioni and Bellotti (2010) has been adopted to simulate the generation of tsunamis by submarine landslides. Essentially, the motion of the sea bottom is provided as a known input to the hydrodynamic equations. The following term is added to the right hand side of the continuity equation:

$$\frac{\partial h_s}{\partial t} \tag{1}$$

where h_s denotes the instantaneous sea surface elevation caused by the transit of the underwater landslide. This term is the link between the landslide model and the tsunami propagation model. The relation between h_s and the local thickness of the slide H_s at the sea bottom is calculated by means of a transfer function according to:

$$\frac{\partial h_s}{\partial t} = \frac{\partial H_s}{\partial t}\frac{1}{\cosh\alpha} \tag{2}$$

with

$$\alpha = \frac{2\pi h}{L_s} \tag{3}$$

Table 1
Fault parameters used in the simulations. Geographical coordinates correspond to the fault center. Rake is 90° in all cases. [1]: Stiros (2010) [2]: Yolsal et al. (2007).

Tsunami	λ_E°	ϕ_N°	Length (km)	Width (km)	Slip (m)	Strike (deg)	Dip (deg)	Reference
F1 (Crete 365 AD)	23.45	35.25	105	100	16	292.5	40	[1]
F2 (Cyprus 1222)	32.50	34.5	50	25	3	305	35	[2]
F3 (Crete 1303)	25.94	34.85	100	30	8	115	45	[2]

where h is the local water depth and L_s is the length of the slide. If the transfer function is not used, then $\partial h_s/\partial t = \partial H_s/\partial t$, which is a good approximation only if the slide length is much larger than the water depth. Using the transfer function $1/\cosh \alpha$ attributes different potential to landslides of different L_s and moving at different ocean depths. As a consequence, a shallow water slide will have a higher capacity of exciting waves ($\alpha \to 0$ and thus $\partial h_s/\partial t \simeq \partial H_s/\partial t$) than if it moves in the deep ocean ($\alpha \gg 0$ and thus $\partial h_s/\partial t \ll \partial H_s/\partial t$) Details are presented in Tinti et al. (2006).

The landslide is described as one body with a prescribed motion due to its slide on a linear slope with a given inclination, as described in detail by Harbitz (1992). However, this description has been slightly modified to account for the more realistic case consisting of two consecutive slides on two different slope inclinations.

The slice starts moving from rest, it reaches a maximum velocity and then decelerates. For the single slope model, Harbitz (1992) proposed a velocity at the slice front which is a sinusoidal function of time. Its amplitude is the maximum velocity, U_{max}, which is obtained as a function of the slope, the average thickness of the slide, its density, the density of turbidity currents, and the friction and drag coefficients. The model description completes by imposing the total horizontal displacement or runout R. The slide velocity is:

$$v = U_{max} sin\left(\frac{\pi t}{T}\right) \quad 0 \le t \le T \tag{4}$$

where the slide duration is:

$$T = \frac{\pi}{2}\frac{R}{U_{max}}. \tag{5}$$

In many cases a first and large slope is involved in the triggering mechanism. After a displacement R_1, the slope decreases, but the moving masses still complete a second displacement R_2. For each slope the maximum velocity $U_{max,1}$ and $U_{max,2}$ are computed as in the previous case, and the following composite velocity profile is imposed:

$$v = U_{max,1} sin\left(\frac{\pi t}{T_1}\right) \quad 0 \le t \le t_{trans} \tag{6}$$

with

$$T_1 = \frac{\pi}{2}\frac{R_1}{U_{max,1}} \tag{7}$$

and

$$v = U_{max,2} sin\left(\frac{\pi}{T_2}(t - t_{trans}) + \frac{\pi}{2}\right) \quad t_{trans} < t \le t_{trans} + \frac{T_2}{2} \tag{8}$$

with

$$T_2 = \frac{\pi[R_1 + R_2 - S(t_{trans})]}{U_{max,2}} \tag{9}$$

where $S(t)$ is the instantaneous position of the slide front at time t and

$$t_{trans} = \frac{T_1}{\pi} arcsin\left(\frac{U_{max,2}}{U_{max,1}}\right). \tag{10}$$

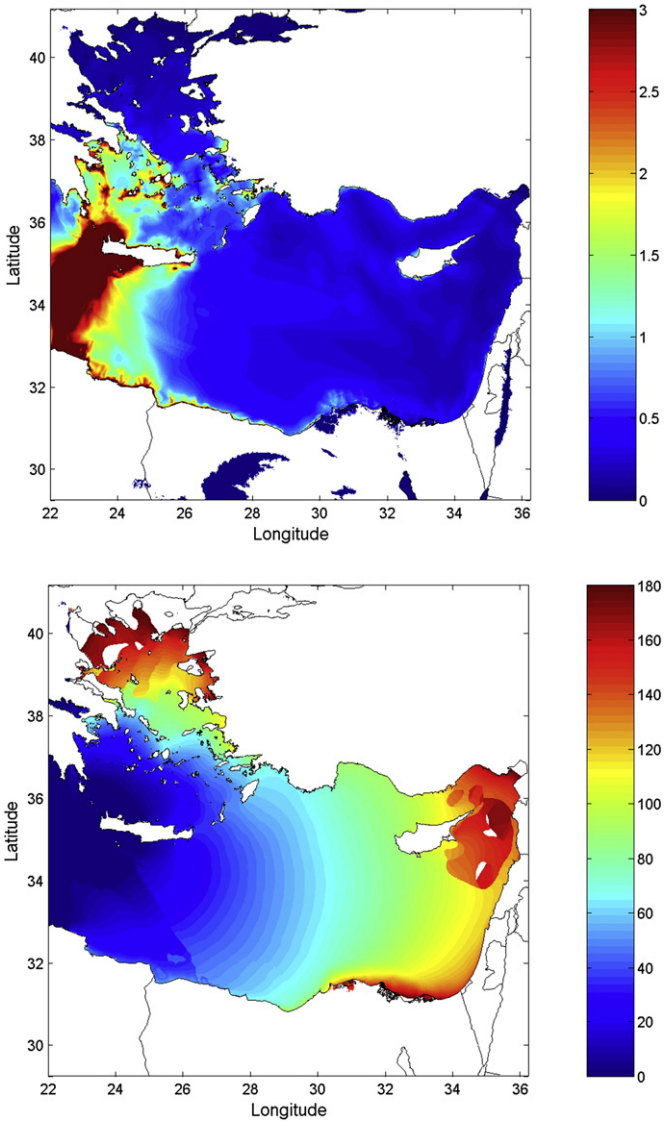

Fig. 2. Results for the Crete 365 AD tsunami after a 3 hour simulation. Top: Calculated wave amplitude (m). Bottom: Arrival times (minutes), defined as time required for the arrival of a signal with 10 cm amplitude.

2.4. Tsunamis generated by a pyroclastic flow into the sea

Essentially this is a particular case of a submarine landslide in which the initial length of the slide is zero and increases in time as the pyroclastic flow is entering the sea. Thus, it is simulated as the submarine landslide case, but changing its length appropriately. In this case the pyroclastic flow enters into the sea at a high initial velocity, U_o, which is imposed as a model parameter. Later, it progressively decreases to zero. The total displacement (R_2) has been estimated as

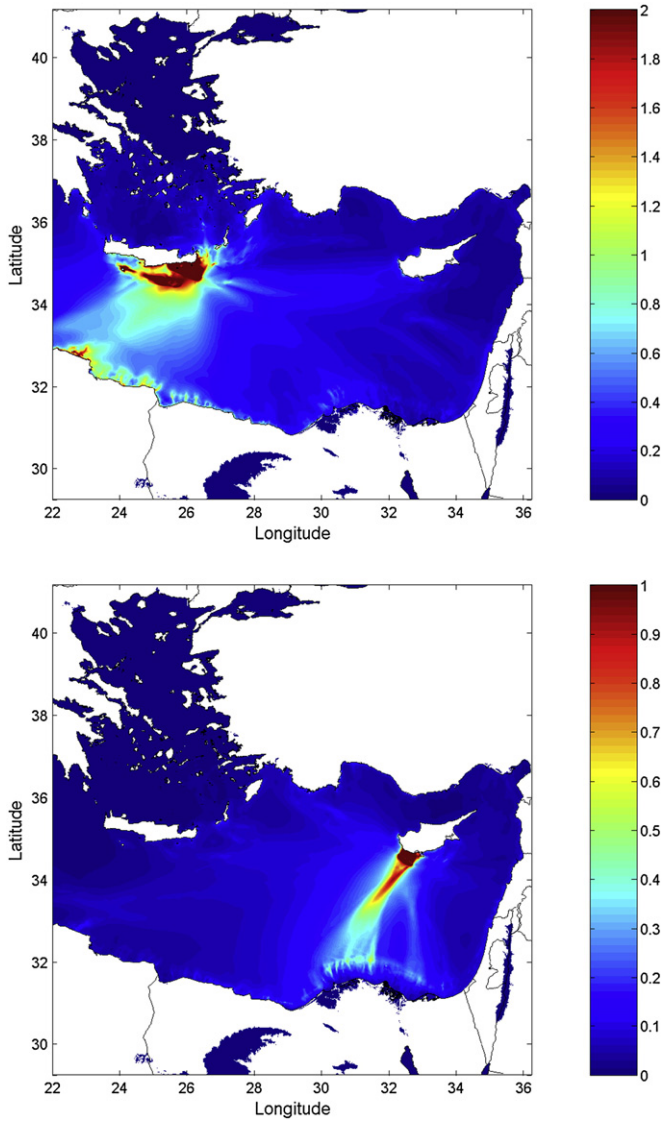

Fig. 3. Calculated wave amplitudes (m) after a 3 hour simulation. Top: Crete 1303 earthquake. Bottom: Cyprus 1222 earthquake.

in Novikova et al. (2011). A reasonable description can then be achieved by setting $t_{trans} = 0$, R_1 and $U_{max,2} = U_o$ in the previous formulation.

3. Simulation of past tsunamis

The model has been implemented in the eastern Mediterranean (Fig. 1) and new generation mechanisms have been incorporated with respect to Periáñez and Abril (2013). Consequently, historic tsunamis occurred in this region have been simulated for a further validation of the model and of the new generation mechanism descriptions.

3.1. Tsunamis produced by earthquakes in geological faults

A number of tsunamis generated in active faults in the eastern Mediterranean have been simulated. Fault parameters are listed in Table 1 and their locations are presented in Fig. 1. Only some results are presented to test model performance, without any discussion on historic facts of events.

3.1.1. Crete, AD365 earthquake

This tsunami has been simulated by a number of authors, and fault parameters may slightly vary among them (Lorito et al., 2008; Yolsal and Taymaz, 2012). Fault parameters in Stiros (2010) have been used in this work (Table 1).

Model results are presented in Fig. 2, which are in good agreement with previous simulations indicated above. It may be seen that energy is mainly directed along a SW direction, as in Lorito et al. (2008). Wave amplitudes are over 4 m along Libya, Crete and in some islands in the Aegean Sea. Although it may not be clearly seen due to the colour scale and large domain, waves in Alexandria (Egypt) reach 2 m, in good agreement with Yolsal and Taymaz (2012).

Calculated arrival times of the tsunami are also in good agreement with Lorito et al. (2008) (Figure 5c in their paper). Thus, they are about 180 min to the northern Aegean Sea, 90 min to Cyprus and some 120 min to the Levantine coast.

3.1.2. Crete, AD1303 earthquake

The magnitude and location of this earthquake is not clear. The source parameters of Yolsal et al. (2007) have been used, although other simulations with a different source have been reported (Hamouda, 2006).

The calculated wave amplitudes are presented in Fig. 3. They are similar to those of Yolsal et al. (2007) and Yolsal and Taymaz (2012). The largest amplitudes are found at the east of Crete, reaching some 5 m here. Relatively large waves also arrive to Libyan coasts (some 1.5 m at some locations).

3.1.3. Cyprus, AD1222 earthquake

Results for this tsunami (calculated wave amplitudes) are presented in Fig. 3. They are in good agreement with the previous calculations in Yolsal et al. (2007). An amplitude of 1 m is obtained along the southern coast of Cyprus, but waves are small over the rest of the domain (a few cm). As in Yolsal et al. (2007), it may be seen that in this case the Nile Delta acts as a natural barrier and slows waves at these shallow depths (<500 m), thus increasing wave amplitude in this area.

3.2. Tsunamis produced by submarine landslides: the Akhziv slide

The 5 × 10 km Akhziv Canyon is located in the Levantine coast, northern Israel (see Fig. 1, L1 source). A landslide scenario occurring

Table 2
Source parameters for tsunamis triggered by submarine landslides. They are defined as in Harbitz (1992) and Eqs. (6)–(10). The direction of the slide (Dir) is measured counterclockwise from east and the position refers to the slide front position. Length (L), width (B) and the smoothing distance in the front and back (S) are measured in km. α is the corresponding slope angle and h_m is the maximum thickness of the slope. The slide volume is calculated from $V = 0.9Bh_m(L + 0.9S)$. The single slope model of Harbitz (1992) has been used for L1, thus some parameters are not relevant in this case.

Slide	Geometrical parameters					Position		Dir	Slope 1			Slope 2		
	L	B	S	h_m (m)	V (km^3)	λ_E°	ϕ_N°	θ°	R_1 (km)	α_1°	$U_{max,1}$ (m/s)	R_2 (km)	α_2°	$U_{max,2}$ (m/s)
L1 (Akhziv)	8	5	8	18.0	1.23	35.05	33.08	135	30.0	–	62.3	–	–	–
L2 (Sirte-1)	16	30	2	22.9	11.0	19.55	32.87	135	18.3	2.5	69.7	32.3	1.2	43.7
L3 (Sirte-2)	16	30	2	22.9	11.0	19.28	31.95	104	50.0	7.0	43.2	102	5.0	8.5
L4 (Alexandria)	20	80	3	6.0	9.8	29.50	31.34	90	11.1	2.8	38.2	14.8	1.5	26.2
L5 (Avaris-a)	32	45	4	6.0	8.7	32.40	32.40	45	7.2	1.7	28.5	50	0.2	6.4
L6 (Avaris-b)	20	80	3	6.0	9.8	32.80	31.66	45	6.3	2.8	38.6	7.7	0.2	7.7

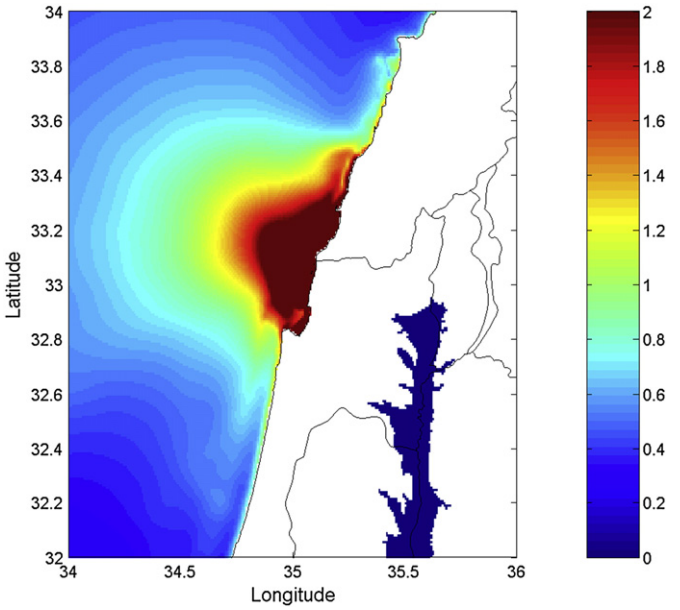

Fig. 4. Calculated wave amplitudes (m) for the Akhziv Canyon landslide (L1) after a 3 hour simulation.

here was proposed by Salamon et al. (2007) and has been simulated. Slide parameters are given in Table 2 (L1). Calculated wave amplitudes are presented in Fig. 4. These are higher than 5 m along the coast in the nearby of the canyon. Significant waves also reach the shore along a 100 km portion of the coast as may be seen in Fig. 4, in agreement with previous calculations (Salamon et al., 2007). Tsunami amplitude decreases rapidly as moving towards the open sea due to the fact that the source area is fairly narrow. Thus, these tsunamis spread faster than those originated from larger earthquake sources.

3.3. Model for caldera collapse: the Late Bronze Age eruption of Santorini

The collapse volume is estimated at 19 to 34 km^3 (Novikova et al., 2011). The simulation carried out for this work used a mean value of 26 km^3, similar to the 24 km^3 of Ozel et al. (2011) and the 25 km^3 of Dominey-Howes (2004). Calculated amplitudes are presented in Fig. 5, which are very similar to those of Ozel et al. (2011) (Figure 8 in their paper). Although the colour scale is limited to 7 m, waves over 10 m high arrive to some islands in the Aegean Sea and to the north coast of Crete. It is interesting to note that, in spite of the strong tsunami produced by the collapse, its effects are limited to the southern Aegean Sea. There is a strong attenuation of waves in the northern Aegean Sea. Also, wave heights in the Eastern Mediterranean are not significant. This is in agreement with the calculations in Ozel et al. (2011) and is due to the strong energy dissipation occurring in the narrow passages between the many small islands existing in the Aegean Sea.

3.4. Tsunamis generated by a pyroclastic flow into the sea: the eruption of Santorini

The same parameters for tsunami generation as in Novikova et al. (2011) have been used. Thus, the pyroclastic flow is assumed to be 55 m thick and 5 km wide with a total volume of 30 km^3. The direction of the flow is 200° measured counterclockwise from north. Computed wave amplitudes are presented in Fig. 5. The colour scale is now limited to 25 m, but 50 m waves reach some locations in the northern coast of Crete. In spite of the strong tsunami, it is again limited to the Aegean Sea as in the caldera collapse case. Indeed, it has already been questioned if Thera tsunami could have reached the Levantine coast (Dominey-Howes, 2004; Salamon et al., 2007).

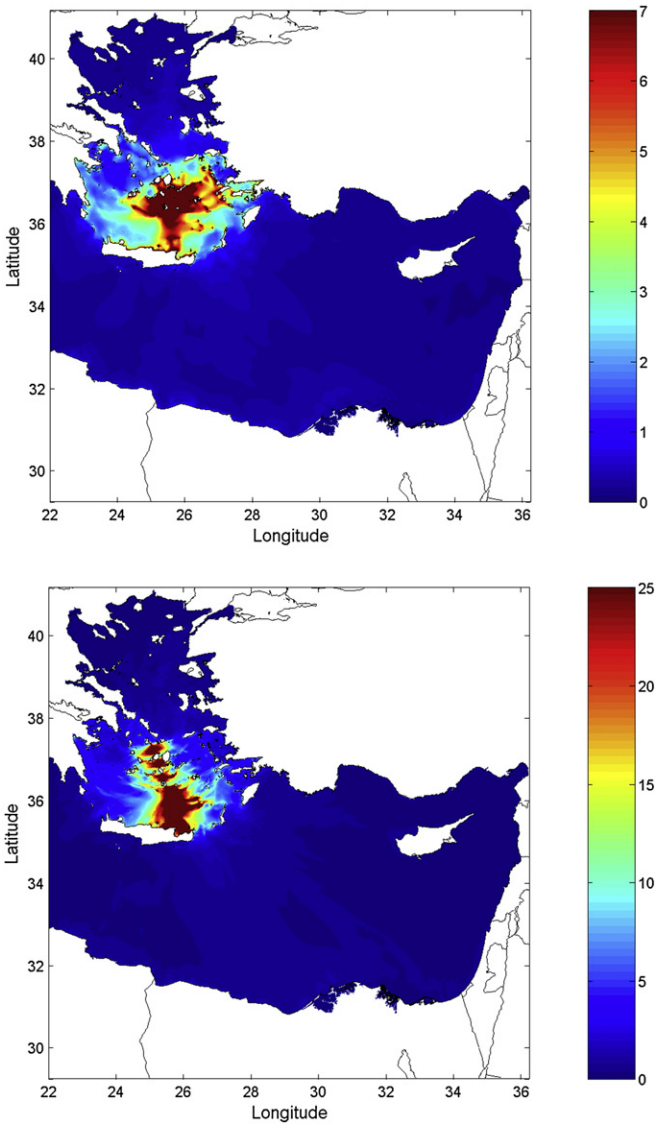

Fig. 5. Calculated wave amplitudes (m) for the LBA Santorini caldera collapse (top) and pyroclastic flow into the sea (bottom) after a 3 hour simulation.

4. The Santorini's tsunami sequence

The previous modelling exercise on the LBA Santorini tsunami triggered by an almost instantaneous caldera collapse has to be considered as being representative of the worst case situation. The model of tsunami generated by the entry of pyroclastic flows may be conservative in terms of the total volume (30 km^3), but the simplifying assumption of a solid block that slowly decelerates, without lateral spreading, tend to overestimate the directional effects. In the present work, model results are reported only for one selected direction (200°) of the slide. Novikova et al. (2011) reported model results for other directions. In the most favourable one, the computed water elevation at Augusta Bay was about 1 m. Thus, it can be concluded that tsunamis produced by the Santorini volcano explosion had produced little effects out of the Aegean Sea. The isochronous (within the range associated to their respective chronologies) tsunamigenic deposits found in distant areas should have been triggered by other sources.

The Augias megaturbidite provides the evidence of giant turbidity currents, likely initialized by a landslide with its associated tsunami. Given the total volume of displaced sediments and their likely source, the numerical simulation of the tsunami can provide some insight on

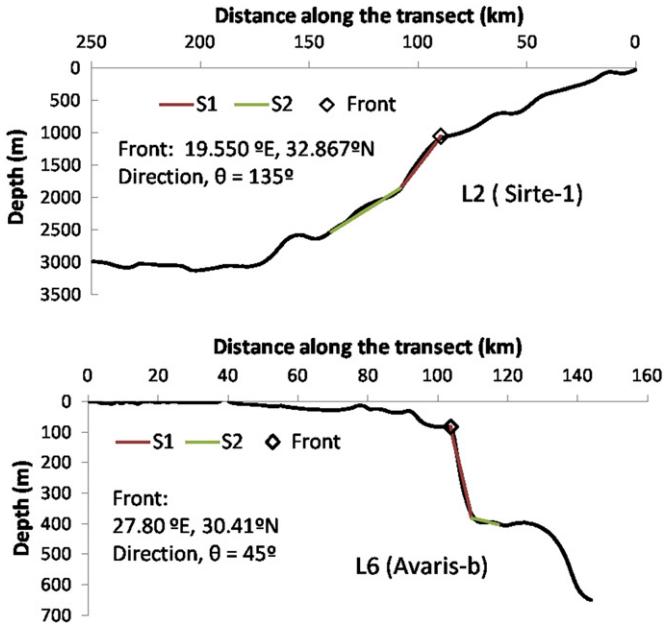

Fig. 6. Depths profiles along the transects (from the shoreline and in the direction of the displacement) along which landslides occurs: a) Sirte-1, and b) Avaris-3. S1 and S2 correspond to the slopes defined in Table 2.

its potential effects over the central Mediterranean area and, particularly, on eastern Sicily (Section 4.1).

In the Israeli coasts, following the argument of Dominey-Howes (2004), the tsunami able to produce the observed deposits of LBA pumice should have been triggered at least few weeks or few months after the Santorini Volcano explosion. Local sources for submarine landslides cannot be discarded, but the particular geological settings of the Nile Delta and the biblical narrative of the sea crossing, as the epilogue of a series of natural disasters, most likely related with the LBA Santorini event, justify the selection of the scenario for the modelling study reported in Section 4.2.

4.1. The Augias megaturbidite

The Santorini earthquake, or the sequence containing it, could have triggered a submarine landslide or gigantic turbidity currents in the African shelf around the Gulf of Sirte, as commented in the Introduction. Some plausible scenarios for the induced tsunami have been modelled.

It is expected that the primary and highest waves were generated during the initial stages of the slide motion, before transition to turbidity current (Harbitz, 1992); thus, the model will focus on a submarine landslide. Cita and Rimoldi (1997), and Hieke and Werner (2000), reported the area covered by the giant homogenite, with a border close to the Western Herodotus Trough, in the African continental shelf. We explored depth profiles along several transects, as those shown in Fig. 6, enabling identification of some candidate locations for slope failures and allowing estimations on direction, displacement and maximum speeds. Finally we adopted some plausible values for geometric parameters of the moving mass, to complete the tsunami source definitions reported in Table 2 (L2 and L3, see Fig. 1 for their locations). A sensitivity test has been conducted to evaluate the effect of variations in the definition of the geometric parameters, as reported just below.

The computed maximum amplitude after 3 h for source Sirte-1 (Table 2) is shown in Fig. 7. When tsunami waves enter the deep central Mediterranean basin, the increase in velocity produces a deflection westwards. This tsunami impacts large coastal areas in northern Africa, western Greece, Malta, eastern Sicilia and SW Italy. Particularly, in eastern Sicilia the tsunami generated waves are above 3 m amplitude,

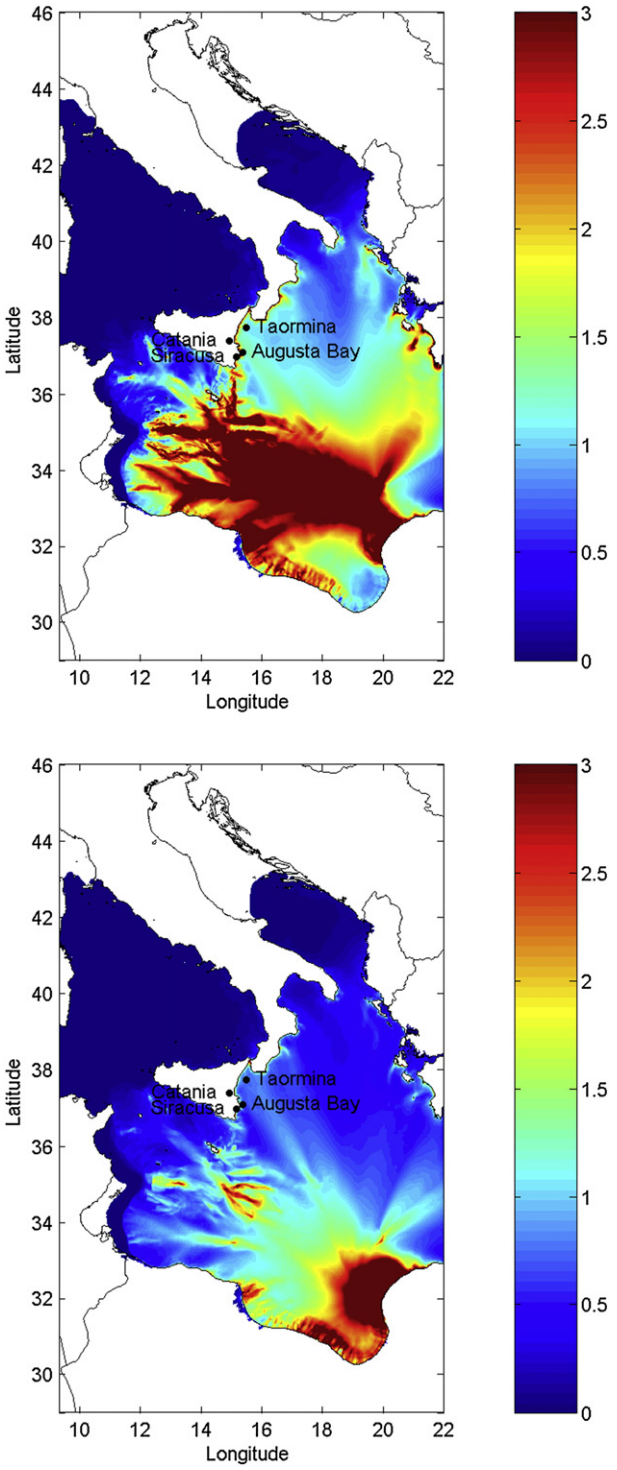

Fig. 7. Computed maximum amplitude (m) after 3 h for the tsunamis generated by landslides Sirte-1 (up) and Sirte-2 (bottom). Landslide parameters are given in Table 2.

as shown in Fig. 8 for a set of locations, including Augusta Bay. Thus, a sequential tsunami like Sirte-1 could have been behind the Augias megaturbidite and the sedimentary deposits, isochronous to the Santorini explosion, that have been reported in Augusta Bay.

Sensitivity tests (not shown) reveal that changes of some 10° in the prescribed slide direction can affect the near field impact of the tsunami. Changes in the shape of the slide, involving only its length and width but preserving its volume, have overall negligible effects. The increase in mean slide height, reducing its length or width, increases the maximum velocity, and consequently the impact intensity, but not its spatial

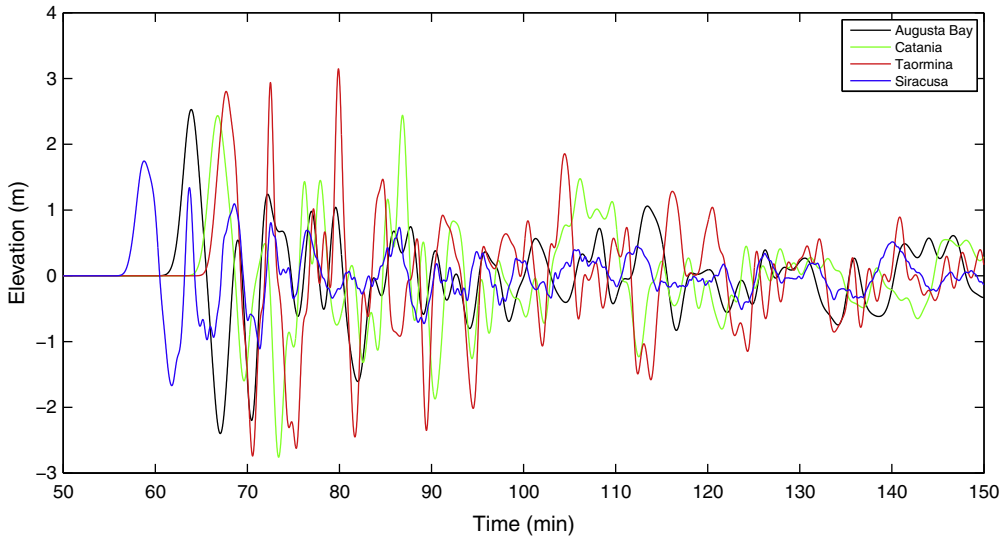

Fig. 8. Calculated time series of water surface elevations (m) in locations indicated in Fig. 7 for Sirte-1 landslide.

distribution. Thus, in the case of Sirte-2, high wave amplitudes are constrained to the slide area, as may be seen in Fig. 7. The impact on Sicilia and SW Italia is much less than in the case of Sirte-1.

4.2. The Nile Delta

4.2.1. Main geological features and tsunamigenic sources

An early study on the nature and evolution of continental shelf sediments in the Nile Delta can be found in Summerhayes et al. (1978), and more recent studies and summaries, among others, in Loncke et al. (2006, 2010), Ducassou et al. (2009), and Prinzhofer and Deville (2013). The first map of the Nile deep-sea fan has not been completed until recent years (Gaullier et al., 2000; Loncke et al., 2006). The geodynamics of the eastern Mediterranean is complex, as explained in the Introduction. A series of fault trends have been identified across the stable shelf of the Nile Delta (e.g. Rosetta, Baltim and Temsah fault trends; Garziglia et al., 2008, and references therein). The Messinian desiccation event led to the deposition of salt and anhydrite throughout the Mediterranean basin, while the proto-Nile river excavated deep canyons and transported offshore large volumes of terrigenous sediments. Thick Plio-Quaternary sediments covered then the ductile evaporitic layers, what triggered some giant gravity-driven salt tectonics (Loncke et al., 2006, 2010). Large-scale slope failures destroyed channel segments and caused the formation of new submarine fan systems. The results of this tectonics can be clearly observed along the borderline that nowadays delimits the stable shelf area from the deep sea fan. The Nile delta is a major gas and condensate province with several mud volcanoes and geodynamics associated to fluid seepage (Bayon et al., 2009; Prinzhofer and Deville, 2013).

Ducassou et al. (2009) published results on the study of the evolution of the Nile deep-sea turbidite system during the Late Quaternary, based upon 42 sediment cores collected across the entire Nile deep-sea fan between 1984 and 2004. Data allowed for palaeogeographic reconstructions covering the period from 200 ka to present. Although they identified several slump deposits and turbidites, the Mid and Late Holocene (ca 5 ka to present) was characterized by a stable sea level, a climatically arid period, low Nile River discharges, and low sedimentation rates (of a few cm ka^{-1}) dominated by carbonate-rich hemipelagic and pelagic muds. It is worth noting that because of the number and the spatial distribution of cores over this huge area, submarine landslides of up to tens of km^3 and moderate run-outs cannot be excluded for this time period. Furthermore, Salamon et al. (2007) reported a historical analysis of earthquakes and tsunamis in the eastern Mediterranean. They found that 10 of the 21 reliably reported tsunamis were clearly associated with on-land earthquakes along the Dead Sea Transform system, likely originated from offshore, seismologically induced slumps.

In the context of the LBA Santorini tsunami, the origin of the energy able to generate the isochronous tsunamigenic deposits found in Israel and Gaza and the way in which the volcano explosion and the subsequent tsunamis could have been behind the history narrated in the Bible remain as open questions.

4.2.2. Palaeographic reconstruction of the Eastern Nile Delta (3500 years BP)

During the last 5 ka, with stable sea level, the major changes in the coastline of the Nile Delta have been driven by fluvial deposits, coastal erosion and land subsidence [this latest estimated as 2.0 mm/year in the area of Alexandria (El-Raey, 1997)]. Coutellier and Stanley (1987), based on a petrological study of numerous sediment borings in the northeastern Nile Delta, with stratigraphic correlation and radiocarbon dating, compiled palaeogeographic maps showing the configuration of the region at different times during the Holocene. They calculated mean Holocene sedimentation rates of 5.0 m/ka. As a result, the coastal margin in the studied area migrated northward by some 50 km during the past 5 ka. The map they reported for the situation at 3500 years BP will serve as a basis for our present study.

The details of the coastline will not significantly affect the general patterns of tsunami propagation, but they are of capital importance for assessing local impacts and for the calculated run-ups. As a practical and crude approach for the reconstruction of the former coastline in the entire Nile Delta at ca 3500 years BP, we followed the methodology applied by Abril et al. (2013) for the former Gulf of Tartessos (SW Spain). Using grid coordinates, we defined two parabolic profiles: the first contains the nowadays coastline, and the second one is displaced southwards, in such a way that the mapped coastline by Coutellier and Stanley (1987) lies between both. Then we applied a correction to the nowadays depths/elevations, linearly decreasing from the upper to the lower parabolas. A correction of 15 m was assigned to the northern parabola in the eastern Nile Delta, linearly decreasing to 10 m in its western area. Correction level was set to zero in the southern parabola. Few further details were manually added to get a final coastline in the eastern Nile Delta quite close to the one proposed by Coutellier and Stanley (1987), as shown in Fig. 10. However, the details of their reconstruction eastern of the nowadays Suez Canal are poor, and they do not contain the more recent findings on the lake shoreline and the palaeolagoon around the ancient Migdol. Nevertheless, this scenario contains the basic features to understand the potential effects of tsunamis. In Fig. 10 the red line plots the coastline, as reconstructed

by Coutellier and Stanley (1987), while the green one corresponds to the limit of the marshland area, which ends in its eastern part in coastal sand ridges. It is worth noting that in the zone of northern Suez Canal, the coastline by Coutellier and Stanley (1987) fits with a land ridge which delimits an area of depressed lands with nowadays elevations still below 1 m.

4.2.3. Modelling tsunamis triggered by submarine landslides in the Nile Delta (3500 years BP)

Garziglia et al. (2008) identified seven mass-transport deposits on the Western province, northern to the Rosetta Canyon, downstream of imbricate scars (30°E, 31.50°N). The estimated volumes ranged from 3 to 500 km^3, mean thickness from 11 to 77 m and runout distances from 18 to 150 km. The dated sediment cores revealed that the youngest deposit took place before the sapropel S1 marker, and then being older than 8940 ± 30 cal. year BP. Concerning the potential causal processes, these authors argue that the presence of gas in the sediment and earthquake shaking may have concurred to trigger large-scale failures on the low slope angles (1°–2°) of the Rosetta area. Loncke et al. (2009) published a general overview on multi-scale slope instabilities along the Nile deep-sea fan. Most of the studied area was surveyed with seismic data of poor resolution, except in its western part, for which high-resolution data were available. The authors were able to classify the instabilities according to their origin (regional salt-tectonics, regional and small sediment failures) and they mapped them over all the studied area. It is worth noting that this study focused on the deep-sea fan area, and that the tracklines of the survey (shown in their Fig. 1) did not cover the stable shelf nor the areas closer to the shoreline. More recently, Ducassou et al. (2013) reported four highly mobile debris flows in the Nile deep-sea fan system, with a chronology confined between 5599 and 6915 cal. years BP for the most recent event, in the Rosetta province.

Recent mass-wasting events can be recognized in bathymetric maps by the presence of head and footwall scars (Loncke et al., 2009). Several candidate sites have been identified along the borderline of the stable shelf area of the Nile Delta, accomplishing for high slopes and being distant enough from the already studied areas, for which any turbidite

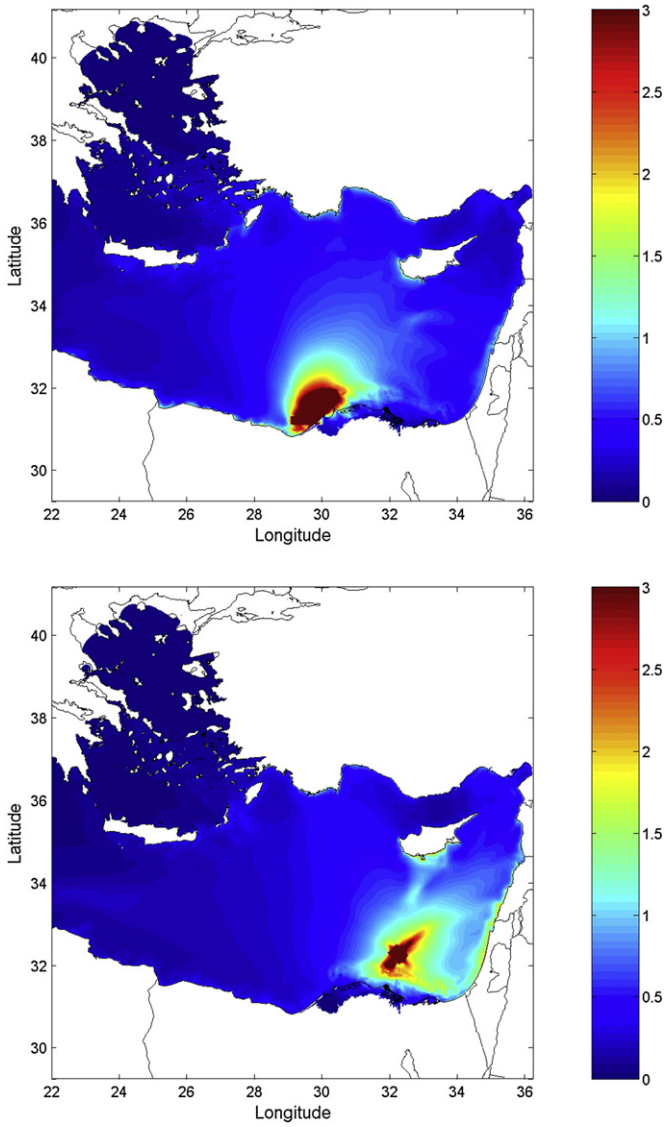

Fig. 9. Computed maximum amplitude (m) after 3 h for the tsunami generated by the landslide Alexandria (up) and Avaris-a (bottom). Landslide parameters are given in Table 2.

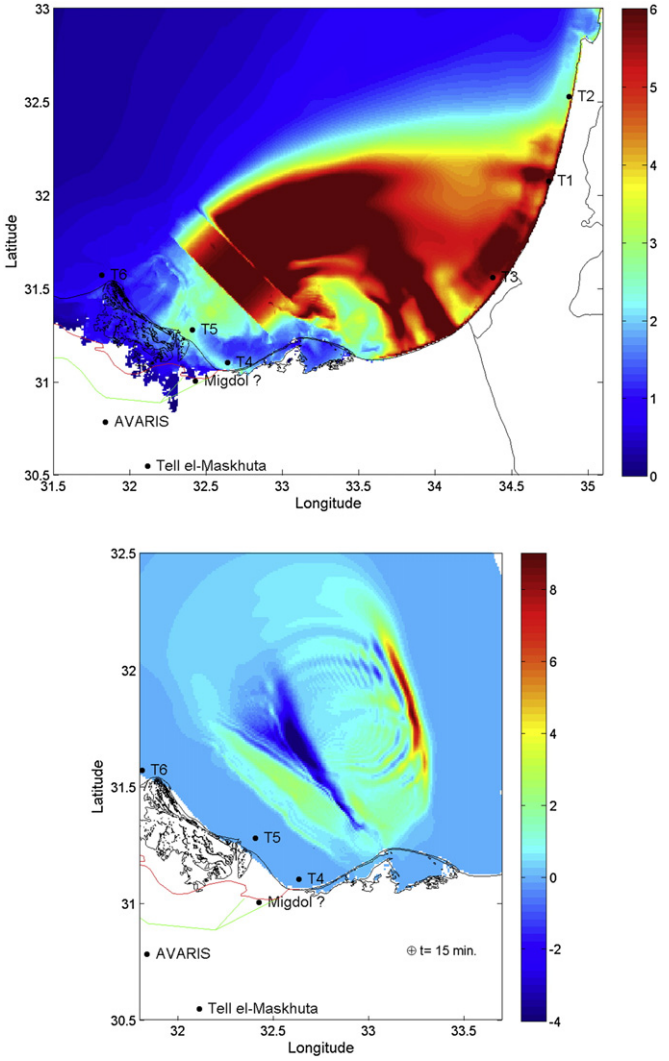

Fig. 10. Computed maximum amplitude (m) after 3 h for the tsunami generated by the landslide Avaris-b (up) and instantaneous water surface elevations 15 min after the slide beginning. Landslide parameters are given in Table 2. The red and green lines indicate, respectively, the former coastline and the limit of marshlands, after Coutellier and Stanley (1987).

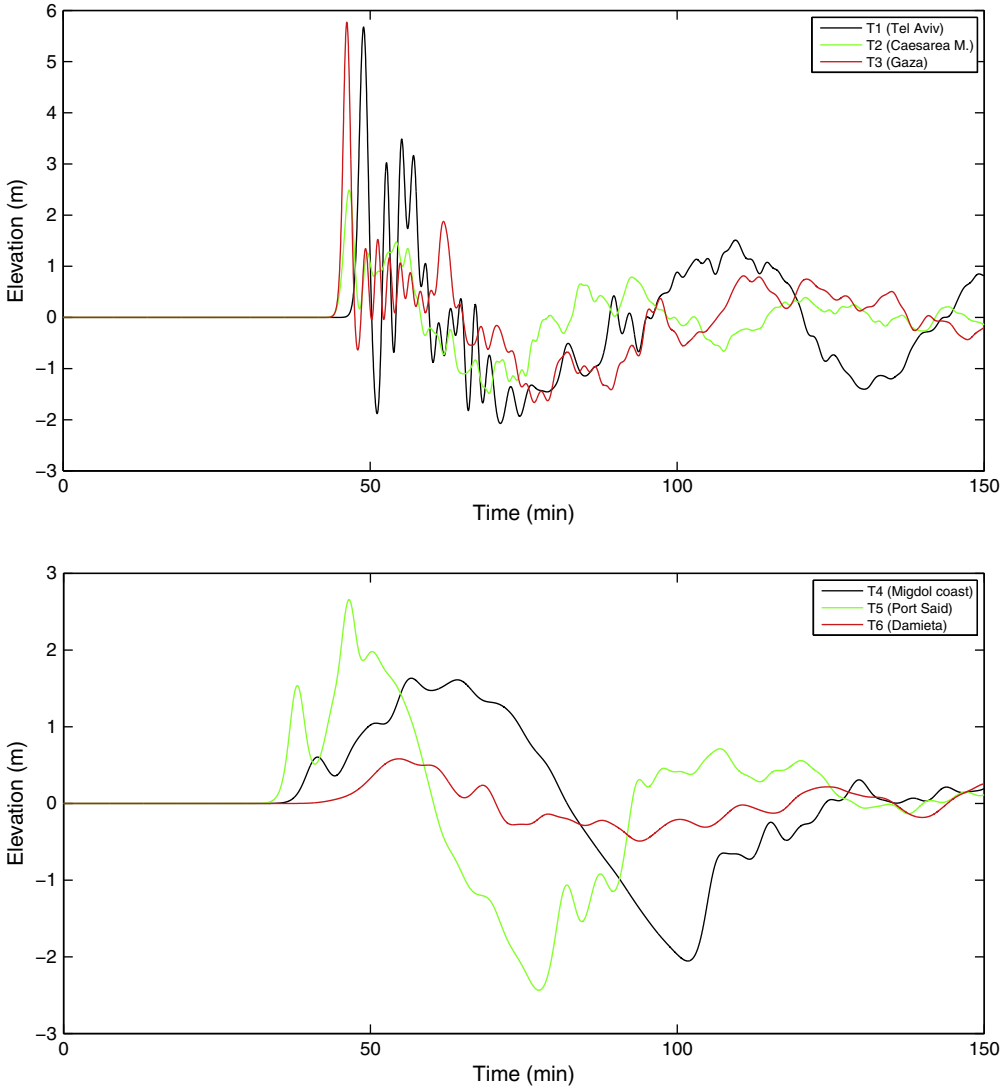

Fig. 11. Calculated time series of water surface elevations (m) in locations indicated in Fig. 10 for *Avaris-b* landslide.

deposits in the last 5 ka can be discarded. The most plausible size for the submarine landslides should be small to moderate, so we selected volumes of ~9–10 km^3. For each location we tried with different combinations of geometrical parameters for the landslide. For the sake of brevity only three sources have been finally selected to support this part of the present study. The corresponding source parameters are shown in Table 2.

Tsunamis generated by landslides of 9–10 km^3 in the western area of the Nile Delta were not able to significantly affect the coastal zones of Israel and Gaza and their effects on the eastern area of the delta were equally negligible. Thus, the source term *Alexandria* in Table 2 will serve to illustrate these results. The source is placed over a long scar which lies east–west, south of the Rosetta branch, and with a typical slope of 2.8°. We note that for this landslide, the end of the prescribed displacement lies 32 km away, and is separated by an intermediate elevation of the seafloor, from the closer sediment core studied (and dated) by Ducassou et al. (2009). Results are shown in Fig. 9 (computed maximum amplitude after 3 h). Although the prescribed runout was directed northwards, the highest amplitudes appear northeast of the source, on the western area of the stable shelf of the Nile Delta.

The source termed *Avaris-a* in Table 2 is placed in the western province of the Nile Delta, mostly characterized by gravity spreading processes which locally create steep escarpments. The front of the landslide was placed at 1000 m depth, at the border of a plateau area that ends in a slope of 1.72°. Results are shown in Fig. 9. The generated tsunami was able to produce waves above 2 m amplitude in the coastal areas of Israel and Gaza, and in southern Cyprus, but it did not propagate southwards into the stable shelf of the Nile Delta, and then, it did not produce any noticeable effects in the coastal areas around the ancient Migdol.

For source *Avaris-b*, the corresponding depth profile along the transect is depicted in Fig. 6. The front of the landslide is placed at the border of the plateau of the stable shelf, at a shallow depth of 100 m. It starts moving down along a slope of 2.82°, over which the slide completes a 6.2 km displacement. This landslide lies close and parallel to the Temsah fault trend (Garziglia et al., 2008). The computed maximum amplitudes after 3 h for the tsunami generated by the landslide *Avaris-b* is shown in Fig. 10. It strongly impacts the coastal areas of Sinai, Israel and Gaza, where waves above 5 m amplitude are registered (Figs. 10 and 11, top). The way in which this tsunami affects the eastern area of the Nile Delta and the surroundings of the ancient Migdol is of particular interest. Fig. 10 shows a snapshot after 15 min of the landslide startup. A wave crest appears at the tsunami front, advancing eastwards. A receding wave, with lower amplitude, moves towards the Damieta and Manzala coasts. Between both, a pronounced depression up to 6 m

deep runs along the breaking line of the landslide, being narrower towards the coastal area. Although hardly observable from the same shoreline, for some exceptional witnesses this phenomenon could remember the division of the waters narrated in Exodus. Due to the shallow waters, the velocity of the tsunami waves over the stable shelf area of the Nile Delta is relatively small. Thus, the trench in the sea surface moves slowly when approaching the coast, until it runs parallel to the shoreline over which it finally breaks (see the sequence of snapshots in Fig. S1, in electronic supplementary material). Fig. 11 shows the computed time series of water elevations in some locations of the ancient coastline of the eastern Nile Delta. These virtual gauges first register the arrival of the recessing front, with a wave amplitude around 2 m. Then waters retire in a slow-moving process, with a decrease in the water level of some 2 m below the local mean sea level. This might have helped the crossing of the coastal isthmus of the palaeolagoon north of Migdol for a not too large group of people. The particular details would depend on the source parameters, but the present modelling exercise is helpful to show that a tsunami generated by a submarine landslide in this area of the Nile Delta, within the time window associated to the Santorini volcano explosion, could have produced the effects observed in the Israel and Gaza coasts, and, at the same time, it includes the basic features that could have inspired the biblical narrative of the Exodus, in which the precursor effects of the Santorini event have been recognized as potential origin of the biblical plagues. Nevertheless, conclusive evidences can only be provided by field studies, particularly by geological surveys intended to identify any fingerprint of eventual submarine landslides having occurring at this place and at that time.

5. Conclusions

A model which simulates the propagation of tsunamis in the central and eastern Mediterranean has been developed. Several tsunami sources have been considered: earthquakes associated with geological faults, submarine landslides, entry of pyroclastic flows into the sea and the collapse of a volcano caldera.

The model performance has been tested through its application to past events and comparing results with previous calculations. Thus, it has been applied to simulate tsunamis induced by Crete AD365 and 1303 earthquakes, Cyprus 1222 earthquake, Akhziv landslide and, finally, Santorini explosion tsunamis produced by caldera collapse and entry of pyroclastic flow in the sea.

The effects of Santorini explosion tsunami on the Mediterranean have been investigated with the model in more detail. It has been confirmed that tsunamis produced by Santorini explosion (due to both caldera collapse and pyroclastic flows) remain confined to the Aegean Sea, with negligible impact outside, in spite of the extremely high waves produced in the Aegean Sea. Thus, geological evidences of this event in Levant coast, Sicily and the Ionian Abyssal Plain should be related to secondary or sequential tsunamis more likely due to submarine landslides which have been triggered by Santorini explosion or by the sequence containing it. In this sense, it has been found that a landslide-induced secondary tsunami in the Gulf of Sirte could have been responsible of the Augias megaturbidite (Ionian Sea) and the sedimentary deposits, isochronous to the Santorini explosion, which have been reported in Augusta Bay (eastern Sicily).

In a similar way, it has been found that a landslide-induced sequential tsunami, occurring in the eastern area of the Nile Delta is able to generate the isochronous tsunamigenic deposits found in Israel and Gaza. The topography of the Nile Delta as it was some 3500 years BP has been reconstructed. Model results for this tsunami include the basic features that could have inspired the biblical narrative of the Exodus, in which the precursor effects of the Santorini event have been recognized as potential origin of the biblical plagues. Nevertheless, conclusive evidences can only be provided by field studies.

References

Abril, J.M., Periáñez, R., Escacena, J.L., 2013. Modeling tides and tsunami propagation in the former Gulf of Tartessos, as a tool for Archaeological Science. J. Archaeol. Sci. 40, 4499–4508.

Barka, A., Reilinger, R., 1997. Active tectonics on the Eastern Mediterranean region: deduced from GPS, neotectonics and seismicity data. Ann. Geofis. XL, 587–610.

Bayon, G., Loncke, L., Dupré, S., Caprais, J.C., Ducassou, E., Duperron, S., Etoubleau, J., Foucher, J.P., Fouquet, Y., Gontharet, S., Henderson, G.M., Huguen, C., Klaucke, I., Mascle, J., Migeon, S., Olu-Le Roy, K., Ondréas, H., Pierre, C., Sibuet, M., Stadnitskaia, A., Woodside, J., 2009. Multi-disciplinary investigation of fluid seepage on an unstable margin: the case of the Central Nile deep sea fan. Mar. Geol. 261, 92–104.

Byers, G.A., 2006. New evidence from Egypt on the location of the Exodus Sea crossing, part 1. Bible Spade 19, 14–22.

Cecioni, C., Bellotti, G., 2010. Modeling tsunamis generated by submerged landslides using depth integrated equations. Appl. Ocean Res. 32, 343–350.

Cioni, R., Gurioli, L., Sbrana, A., Vougioukalakis, G., 2000. Precursors to the Plinian eruptions of Thera (Late Bronze Age) and Vesuvius (AD 79): data from archaeological areas. Phys. Chem. Earth A 25, 719–724.

Cita, M.B., Rimoldi, B., 1997. Geological and geophysical evidence for the Holocene tsunami deposit in the eastern Mediterranean deep-sea record. J. Geodyn. 24, 293–304.

Cita, M.B., Camerlenghi, A., Rimoldi, B., 1996. Deep-sea tsunami deposits in the eastern Mediterranean: new evidence and depositional models. Sediment. Geol. 104 (1–4), 155–173.

Coutellier, V., Stanley, D.J., 1987. Late quaternary stratigraphy and paleogeography of the eastern Nile Delta, Egypt. Mar. Geol. 77, 257–275.

De Martini, P.M., Barbano, M.S., Smedile, A., Gerardi, F., Pantosti, D., Del Carlo, P., Pirrotta, C., 2010. A unique 4000 year long geological record of multiple tsunami inundations in the Augusta Bay (eastern Sicily, Italy). Mar. Geol. 276, 42–57.

De Martini, P.M., Barbano, M.S., Pantosti, D., Smedile, A., Pirrotta, C., Del Carlo, P., Pinzi, S., 2012. Geological evidence for paleotsunamis along eastern Sicily (Italy): an overview. Nat. Hazards Earth Syst. Sci. 12, 2569–2580.

Dominey-Howes, D., 2004. A re-analysis of the Late Bronze Age eruption and tsunami of Santorini, Greece, and the implications for the volcano-tsunami hazard. J. Volcanol. Geotherm. Res. 130, 107–132.

Ducassou, E., Migeon, S., Mulder, T., Murat, A., Capotondi, L., Bernasconi, S.M., Macle, J., 2009. Evolution of the Nile deep-sea turbidite system during the Late Quaternary: influence of climate change on fan sedimentation. Sedimentology 56, 2061–2090.

Ducassou, E., Migeon, S., Capotondi, L., Mascle, J., 2013. Run-out distance and erosion debris-flows in the Nile deep-sea fan system: evidence from lithofacies and micropaleontological analyses. Mar. Pet. Geol. 39, 102–123.

El-Raey, M., 1997. Vulnerability assessment of the coastal zone of the Nile delta of Egypt, to the impacts of sea level rise. Ocean Coast. Manag. 37, 29–40.

Friedrich, W.L., 2013. The Minoan Eruption of Santorini around 1613 B.C. and its consequences. Tagung en des Landesmuseums für Vorges chichte Halle. Band 9, 37–48.

Galli, P., 2000. New empirical relationships between magnitude and distance for liquefaction. Tectonophysics 324, 169–187.

Garziglia, S., Migeon, S., Ducassou, E., Loncke, L., Macle, J., 2008. Mass-transport deposits on the Rosetta province (NW Nile deep-sea turbidite system, Egyptian margin): characteristics, distribution, and potential causal processes. Mar. Geol. 250, 180–198.

Gaullier, V., Mart, Y., Bellaiche, G., Macle, J., Vendeville, B., Zitter, T., Prismed II scientific parties, 2000. Salt tectonics in and around the Nile Deep-Sea Fan: insights from the PRISMED II cruise: from the Artic to the Mediterranean: salt, shale and igneous diapirs in and around Europe. Geol. Soc. 174, 111–129.

Goodman-Tchernov, B.N., Dey, H.W., Reinhardt, E.G., McCoy, F., Mart, Y., 2009. Tsunami waves generated by the Santorini eruption reached Eastern Mediterranean shores. Geology 37, 943–946.

Hamouda, A.Z., 2006. Numerical computations of 1303 tsunamigenic propagation towards Alexandria, Egyptian Coast. J. Afr. Earth Sci. 44, 37–44.

Harbitz, C.B., 1992. Model simulations of tsunamis generated by the Storegga slides. Mar. Geol. 105, 1–21.

Herzfeld, M., Schmidt, M., Griffies, S.M., Liang, Z., 2011. Realistic test cases for limited area ocean modelling. Ocean Model. 37, 1–34.

Hieke, W., 1984. A thick Holocene homogenite from the Ionian Abyssal Plain (Eastern Mediterranean). Mar. Geol. 55, 63–78.

Hieke, W., Werner, F., 2000. The Augias megaturbidite in the central Ionian Sea (central Mediterranean) and its relation to the Holocene Santorini event. Sediment. Geol. 135, 205–218.

Hoffmeier, J.K., 2005. Ancient Israel in Sinai. Oxford University, New York.

Ioualalen, M., Arreaga-Vargas, P., Pophet, N., Chlieh, M., Ilayaraja, K., Ordoñez, J., Renteria, W., Pazmiño, N., 2010. Numerical modelling of the 26th December 2004 Indian Ocean tsunami for the southeastern coast of India. Pure Appl. Geophys. 167, 1205–1214.

Kampf, J., 2009. Ocean Modelling for Beginners. Springer-Verlag, Heidelberg.

Kowalik, Z., Murty, T.S., 1993. Numerical Modelling of Ocean Dynamics. World Scientific, Singapore.

Lima, V.V., Miranda, J.M., Baptista, M.A., Catalão, J., Gonzalez, M., Otero, L., Olabarrieta, M., Álvarez-Gómez, J.A., Carreño, E., 2010. Impact of a 1755-like tsunami in Huelva, Spain. Nat. Hazards Earth Syst. Sci. 10, 139–148.

Loncke, L., Gaullier, V., Macle, J., Vendeville, B., Camera, L., 2006. The Nile deep-sea fan: an example of interacting sedimentation, salt tectonics, and inherited subsalt paleotopographic features. Mar. Pet. Geol. 23, 297–315.

Loncke, L., Gaullier, V., Droz, L., Ducassou, E., 2009. Multi-scale slope instabilities along the Nile deep-sea fan, Egyptian margin: A general overview. Marine and Petroleum Geology 26, 633–646.
Loncke, L., Vendeville, B.C., Gaullier, V., Mascle, J., 2010. Respective contributions of tectonic and gravity-driven processes on the structural pattern in the Eastern Nile deep-sea fan: insights from physical experiments. Basin Res. 22, 765–782.
Lorito, S., Tiberti, M.M., Basili, R., Piatanesi, A., Valensise, G., 2008. Earthquake-generated tsunamis in the Mediterranean Sea: scenarions of potential threats to Southern Italy. J. Geophys. Res. 113, B1301 (14 pp.).
Mascle, J., Benkhelil, J., Bellaiche, G., Zitter, T., Woodside, J., Loncke, L., Prismed II Scientific Party, 2000. Marine geologic evidence for a Levantine-Sinai Plate; a new piece of the Mediterranean puzzle. Geology (Boulder) 28 (9), 779–782.
Mészáros, S., 1978. Some words on the Minoan tsunami of Santorini. In: Doumas, C. (Ed.), Thera and the Aegean World II. The Thera Foundation, London, pp. 257–262.
Neev, D., Balker, N., Emery, K.O., 1987. Mediterranean Coast of Israel and Sinai, Holocene Tectonics from Geology and Geophysics and Archaeology. Taylor and Francis, New York, p. 130.
Nomanbhoy, N., Satake, K., 1995. Generation mechanism of tsunamis from the 1883 Krakatau eruption. Geophys. Res. Lett. 22, 509–512.
Novikova, T., Papadopoulos, G.A., McCoy, F.W., 2011. Modelling of tsunami generated by the giant Late Bronze Age eruption of Thera, South Aegean Sea, Greece. Geophys. J. Int. 186, 665–680.
Nur, A., Cline, E.H., 2000. Poseidon's horses: plate tectonics and earthquake storms in the Late Bronze Age Aegean and Eastern Mediterranean. J. Archaeol. Sci. 27, 43–63.
Okada, Y., 1985. Surface deformation due to shear and tensile faults in a half-space. Bull. Seismol. Soc. Am. 75, 1135–1154.
Ozel, N.M., Ocal, N., Cevdet, Y.A., Dogan, K., Mustafa, E., 2011. Tsunami hazard in the Eastern Mediterranean and its connected seas: towards a tsunami warning center in Turkey. Soil Dyn. Earthq. Eng. 31, 598–610.
Papathanassiou, G., Pavlides, S., Christaras, B., Pitilakis, K., 2005. Liquefaction case histories and empirical relations of earthquake magnitude versus distance from the boarder Aegean region. J. Geodyn. 40, 257–278.
Periáñez, R., Abril, J.M., 2013. Modelling tsunami propagation in the Iberia-Africa plate boundary: historical events, regional exposure and the case-study of the former Gulf of Tartessos. J. Mar. Syst. 111–112, 223–234.
Pfannenstiel, M., 1960. Erlauterungen zu den bathymetrischen Karten des ostlichen Mittelmeeres. Bull. Inst. Oceanogr. 1192.
Polonia, A., Bonatti, E., Camerlenghi, A., Lucchi, R.G., Panieri, G., Gasperini, L., 2013. Mediterranean megaturbidite triggered by the AD 365 Crete earthquake and tsunami. Sci. Rep. 3 (1285), 1–12. http://dx.doi.org/10.1038/srep01285.
Prinzhofer, A., Deville, E., 2013. Origins of hydrocarbon gas seeping out from offshore mud volcanoes in the Nile delta. Tectonophysics 591, 52–61.
Sahal, A., Roger, J., Allgeyer, S., Lemaire, B., Hebert, H., Schindelé, F., Lavigne, F., 2009. The tsunami triggered by the 21 May 2003 Boumerdes-Zmmouri (Algeria) earthquake: field investigations on the French Mediterranean coast and tsunami modelling. Nat. Hazards Earth Syst. Sci. 9, 1823–1834.
Salamon, A., Rockwell, T., Ward, S.N., Guidoboni, E., Comastri, A., 2007. Tsunami hazard evaluation of the Eastern Mediterranean: historical analysis and selected modelling. Bull. Seismol. Soc. Am. 97, 705–724.
Shiki, T., Cita, B., 2008. Tsunami-related sedimentary properties of Mediterranean homogenites as an example of deep-sea Tsunamiite. In: Shiki, E.T., Tsuji, Y., Minoura, K., Yamazaki, T. (Eds.), Tsunamiites and Implications. Elsevier B.V., pp. 203–215.
Sigurdsson, H., Carey, S., Alexandri, M., Vougioukalakis, G., Croff, K., Roman, C., Sakellariou, D., Anagnostou, C., Rousakis, G., Ioakim, C., Gogou, A., Ballas, D., Misaridis, T., Nomikou, P., 2006. Marine investigations of Greece's Santorini volcanic field. Eos 87 (34), 337–339.
Stanley, D.J., Sheng, J., 1986. Volcanic shards from Santorini (Upper Minoan ash) in the Nile Delta, Egypt. Nature 320, 733–735.
Stiros, S.C., 2010. The 8.5+ magnitude AD365 earthquake in Crete: coastal uplift, topography changes, archaeological and historical signature. Quat. Int. 216, 54–63.
Summerhayes, C.P., Sestini, G., Misdorp, R., Marks, N., 1978. Nile Delta: nature and evolution of continental shelf sediments. Mar. Geol. 27, 43–65.
Tinti, S., Armigliato, A., Pagnoni, G., Zaniboni, F., 2005. Scenarions of giant tsunamis of tectonic origin in the Mediterranean. ISET J. Earthq. Technol. 42, 171–188.
Tinti, S., Pagnoni, G., Zaniboni, F., 2006. The landslides and tsunamis of the 30th of December 2002 in Stromboli analyzed through numerical simulations. Bull. Volcanol. 68, 462–479.
Trevisanato, S.I., 2006a. Treatments for burns in the London Medical Papyrus show the first seven biblical plagues of Egypt are coherent with Santorini's volcanic fallout. Med. Hypotheses 66, 193–196.
Trevisanato, S.I., 2006b. Six medical papyri describe the effects of Santorini's volcanic ash, and provide Egyptian parallels to the so-called biblical plagues. Med. Hypotheses 67, 187–190.
Trevisanato, S.I., 2007. Medical papyri describe the effects of the Santorini eruption on human health, and date the eruption to August 1603–March 1601 BC. Med. Hypotheses 68, 446–449.
Troelstra, S., 1987. Late quaternary sedimentation in the Tyro and Kretheus Bassins, southeast of Crete. Mar. Geol. 75, 77–91.
Yolsal, S., Taymaz, T., 2012. Earthquake source parameters along the Hellenic subduction zone and numerical simulations of historical tsunamis in the Eastern Mediterranean. Tectonophysics 536–537, 61–100.
Yolsal, S., Taymaz, T., Yalciner, A.C., 2007. Understanding tsunamis, potential source regions and tsunami-prone mechanisms in the Eastern Mediterranean. Geol. Soc. Lond., Spec. Publ. 291, 201–230.